Inhibition of the Complement Alternative Pathway by Chemically Modified DNA Aptamers That Bind with Picomolar Affinity to Factor B

Xin Xu,*[,1] Chi Zhang,[†,1] Dalton T. Denton,* Daniel O'Connell,[‡] Daniel W. Drolet,[†] and Brian V. Geisbrecht*

The complement system is a conserved component of innate immunity that fulfills diverse roles in defense and homeostasis. Inappropriate activation of complement contributes to many inflammatory diseases, however, which has led to a renewed emphasis on development of therapeutic complement inhibitors. Activation of complement component C3 is required for amplification of complement and is achieved through two multisubunit proteases called C3 convertases. Of these, the alternative pathway (AP) C3 convertase is responsible for a majority of the C3 activation products in vivo, which renders it an attractive target for inhibitor discovery. In this study, we report the identification and characterization of two related slow off-rate modified DNA aptamers (SOMAmer) reagents that inhibit formation of the AP C3 convertase by binding to the proprotease, factor B (FB). These aptamers, known as SL1102 (31 bases) and SL1103 (29 bases), contain uniform substitutions of 5-(*N*-2-naphthylethylcarboxyamide)-2′-deoxyuridine for deoxythymidine. SL1102 and SL1103 bind FB with K_d values of 49 and 88 pM, respectively, and inhibit activation of C3 and lysis of rabbit erythrocytes under AP-specific conditions. Cocrystal structures of SL1102 (3.4 Å) and SL1103 (3.1 Å) bound to human FB revealed that SL1102 and SL1103 recognize a site at the juncture of the CCP1, CCP3, and vWF domains of FB. Consistent with these structures and previously published information, these aptamers inhibited FB binding to C3b and blocked formation of the AP C3 convertase. Together, these results demonstrate potent AP inhibition by modified DNA aptamers and expand the pipeline of FB-binding molecules with favorable pharmacologic properties. ***The Journal of Immunology*****, 2021, 206: 861–873.**

Complement is an ancient and evolutionarily conserved branch of the innate immune system that makes numerous contributions to human health and disease (1, 2). Although complement is best known for its ability to recognize and facilitate elimination of invading microorganisms, roles for complement in coordinating the overall immune response in repairing damaged tissue and in promoting developmental processes are now widely understood (1, 2). In recent years, complement has received considerable attention owing to a growing appreciation of its links to a number of prominent diseases, such as cancer and Alzheimer disease (reviewed in Ref. 3–7). This has spurred a renewed interest in the discovery of complement-targeted therapeutics, with many such candidates moving through various stages of (pre-)clinical development (8).

Complement activity has traditionally been thought to arise from three different pathways (1, 2). However, contemporary evidence suggests that these are better viewed as two initiation routes (i.e., the classical pathways [CP] and lectin pathways [LP]) and an amplification system (i.e., the alternative pathway [AP]) (1, 2). The CP and LP use distinct pattern recognition molecules to recognize surface-bound Ig molecules and carbohydrates, respectively, and trigger the activation of pathway-specific proteases (i.e., C1s and MASP-1/2) that cleave complement component C4. The activated form of C4, called C4b, is covalently deposited on nearby surfaces, where it binds the proprotease C2 in an Mg^{2+}-dependent manner. Once C4b-bound C2 is cleaved by the pathway-specific proteases mentioned above, it forms a metastable enzyme known as the CP/LP C3 convertase (i.e., C4b2a) that cleaves the next component in the pathway, C3. The activated form of C3, called C3b, is also deposited on the surface and forms an Mg^{2+}-dependent complex with a separate proprotease, factor B (FB). Once C3b-bound FB is cleaved by factor D (FD), it forms another metastable enzyme known as the AP C3 convertase (i.e., C3bBb). Although not explicitly required for AP C3 convertase formation or function,

*Department of Biochemistry and Molecular Biophysics, Kansas State University, Manhattan, KS 66506; [†]SomaLogic, Inc., Boulder, CO 80301; and [‡]St. Andrew's School, Middletown, DE 19709

[1]X.X. and C.Z. contributed equally to this study.

ORCIDs: 0000-0002-0728-0821 (X.X.); 0000-0002-1877-0092 (D.W.D.).

Received for publication November 5, 2020. Accepted for publication December 8, 2020.

This work was supported by the National Institute of Allergy and Infectious Diseases, National Institutes of Health Grant AI113552 and National Institute of Neurological Disorders and Stroke, National Institutes of Health Grant NS104767 (both to B.V.G.).

The crystallographic structures presented in this article have been submitted to the Research Collaboratory for Structural Bioinformatics Protein Data Bank (http://wwpdb.org/) under accession numbers 7JTN and 7JTQ.

Address correspondence and reprint requests to Dr. Brian V. Geisbrecht, Kansas State University, 141 Chalmers Hall, 1711 Claflin Road, Manhattan, KS 66506. E-mail address: geisbrechtb@ksu.edu

The online version of this article contains supplemental material.

Abbreviations used in this article: AF, Alexa Fluor 488; AP, alternative pathway; CI, confidence interval; CP, classical pathway; dT, deoxythymidine; FB, factor B; fc, flow cell; FD, factor D; FH, factor H; GVB, gelatin veronal buffer; LP, lectin pathway; 2NEdU, 5-(*N*-2-naphthylethylcarboxyamide)-2′-deoxyuridine; NHS, normal human serum; 2′-OMe, 2′-*O*-methyl ribose; PDB, Protein Data Bank; RU, resonance unit; SELEX, systematic evolution of ligands by exponential enrichment; SOMAmer, slow off-rate modified aptamer; SPR, surface plasmon resonance; vWF, von Willebrand factor.

C3bBb can be further stabilized by the positive regulatory protein properdin. In this manner, the AP C3 convertase provides a powerful means for complement self-amplification as it generates additional C3b molecules from native C3. Indeed, although both forms of C3 convertase subsequently cleave C5 (9, 10), studies have shown that the AP C3 convertase provides more than 80% of the downstream products that culminate in effector function (11, 12). This strongly suggests that any molecules that perturb AP C3 convertase formation and/or function should be powerful inhibitors of complement activity.

Extensive structural and biochemical analyses have provided a wealth of insight into the formation, function, and regulation of the AP C3 convertase (reviewed in Ref. 13). These have revealed numerous details on the protein–protein interactions, proteolytic reactions, and conformational transitions that are required to generate enzymatically active C3bBb from its molecular precursors. The existence of no fewer than 10 individual steps in this process underscores the size and complexity of the proteins involved, as well as the need to strictly control both the levels and activity of the AP C3 convertase in vivo (13). Although each of these steps theoretically provides a potential point for regulatory fine-tuning of the overall process, the most well-understood AP regulatory strategies manifest through C3b-binding molecules that influence two key events. In this regard, the primary endogenous inhibitor of the AP is the C3b-binding protein factor H (FH) (13, 14). FH not only dissociates the active convertase (i.e., decay accelerating activity) but also prevents formation of new convertases by stimulating the proteolytic degradation of C3b to iC3b by factor I (i.e., cofactor activity). Exogenous C3b-binding molecules that inhibit AP C3 convertase formation and function have also been identified and characterized. Among these are the mAb and 3E7/H17 (15) and the innate immune evasion proteins Efb (16, 17), Ehp (18), and SCINs (19–22) from the Gram-positive pathogen *Staphylococcus aureus*. Collectively, these molecules employ various ortho- and allosteric mechanisms to impair convertase formation by either blocking FB binding to C3b and/or preventing cleavage of the C3 substrate. These observations provide proof of concept that AP C3 convertase regulatory modes distinct from those typified by FH are achievable by macromolecules.

The structural and functional properties of FB itself also contribute to AP regulation by influencing the opposing processes of AP C3 convertase formation and decay. Human FB is an ~93-kDa protein comprised of five independently folding domains that give rise to two functionally discrete regions denoted Ba and Bb (23). The Ba region (~30 kDa) accounts for roughly one third of the molecule and is comprised of the first three domains, each of which adopts the canonical complement control protein fold (CCP1–CCP3). The Bb region (~60 kDa) accounts for roughly two thirds of the molecule and is comprised of the latter two domains. The first of these is a von Willebrand factor (vWF) domain, which contributes the metal ion–dependent adhesion site (MIDAS) that coveys the Mg^{2+} dependence of the AP. The second is a serine protease (SP) domain that provides the catalytic machinery of the enzyme. Association of FB with C3b involves both Ba and Bb regions (24), although their contributions are mechanistically distinct (17, 22, 24, 25). Whereas Ba contributes an initial fast association event that can be measured with Ba fragment alone or FB in the absence of divalent cations, Bb contributes the slower association event that is Mg^{2+} dependent. Significantly, this latter reaction cannot occur on its own and must be coupled to the initial Ba-dependent event; this gives rise to an essential regulatory feature of the AP C3 convertase. Crystallographic studies of FB both free (23) and bound to C3b (25) have revealed the molecular details of the separate Ba and Bb contact sites with C3b. They have also highlighted key conformational transitions that FB undergoes that render it susceptible to cleavage and activation by FD only when in the C3b-bound state (23, 25). Thus, the surprisingly complex series of events that underlie FB binding to C3b and its subsequent activation by FD suggest that this process could be exploited for inhibitor development.

Aptamers are single-stranded nucleic acid ligands directed against other molecules (26). They can be identified from combinatoric libraries of tremendous initial diversity through a process known as systematic evolution of ligands by exponential enrichment (SELEX) (27, 28). Although aptamers recognize their ligands with specificity, the paucity of hydrophobic groups present in conventional nucleotides has been an impediment to aptamers obtaining the high affinities characteristic of tightly binding protein–protein interactions (26). To address this limitation, modified nucleotide bases with functional groups reminiscent of hydrophobic amino acid sidechains have been developed and employed in SELEX strategies (29, 30). A large panel of aptamers with significantly improved affinities for their cognate ligands has since been identified using this approach (29). Owing to their unique physicochemical properties, this new class of aptamers has been given the name slow off-rate modified aptamers (SOMAmer) reagents. In addition to their improved affinities, these reagents can also be synthesized with 2′-*O*-methyl groups or 3′–3′ inverted linkages; these modifications can increase the chemical stability of the aptamers in complex mixtures like serum by impairing degradation by nucleases. As such, aptamers of this sort may represent a valuable tool for developing therapeutic inhibitors of complement proteins, many of which are serum resident.

In this study, we identify and characterize structurally two sequence-related SOMAmer reagents that bind to human FB and potently inhibit functional assays specific for the AP. These molecules, known as SL1102 and SL1103, contain 31 and 29 bases, respectively, and incorporate the unconventional nucleoside 5-(*N*-2-naphthylethylcarboxyamide)-2′-deoxyuridine (2NEdU) in lieu of deoxythymidine (dT) (31). Four of the seven 2NEdU found in these aptamers are especially required for high-affinity binding to FB, as judged by analysis of synthetic dT analogues. Crystal structures of SL1102 and SL1103 bound to FB demonstrate that the aptamers recognize a motif lying at the juncture of the CCP1, CCP3, and vWF domains of the proprotease. This prevents FB binding to C3b and formation of the AP C3 convertase. These results not only provide a unique description of complement inhibition by aptamers, they also increase our understanding of the relationship between nucleic acid ligand structure and function.

Materials and Methods

Materials

Unless otherwise stated, proteins, zymosan A, and erythrocyte preparations were obtained from Complement Technologies (Tyler, TX). Sera for various assays were obtained from either Complement Technologies or Innovative Research (Novi, MI). Human FB that had been purified from human serum was obtained from both Complement Technologies and Quidel (San Diego, CA).

Protein labeling

Native human FB (Quidel) was labeled via primary amines with either Alexa Fluor 488 (AF; Molecular Probes) or biotin (EZ-Link NHS-PEG_4-Biotin; Pierce) according to manufacturer's directions. Briefly,

FB (400 pM in 75 μl) was incubated for 16 h at 4°C with a 22-fold (AF) or 10-fold (NHS-PEG_4-Biotin) molar excess of reagent. Unreacted label was removed by ultrafiltration using Ultracel 3 kDa filters (MilliporeSigma) and buffer solution SB18T0.01 (40 mM HEPES [pH 7.5], 102 mM NaCl, 5 mM $MgCl_2$, 5 mM KCl, and 0.01% [v/v] Tween 20).

Modified aptamer discovery and sequencing

Aptamer selection, with minor modifications, was performed using the SELEX process as described elsewhere (29) using a DNA library 5′-B-B-TTTTTTTTCCTTTCCTTGTTCTGTTGTTG-$(N)_{40}$-CAAGGTAG-GTCGGCGTCACT that included 40 consecutive random nucleotide positions [$(N)_{40}$] and two 5′ biotins (B). The random region contained the modified nucleotide 2NEdU in place of dT. Flanking regions served as templates for amplification by PCR. Ten rounds of SELEX were performed using AF-labeled FB for rounds 1–4 and biotin-labeled FB for rounds 5–10. Binding steps were performed at 37°C in buffer solution SB18T0.01, as described above. Incubation time was 60 min for round 1 and 15 min for all subsequent rounds. Approximate FB concentrations were 500 nM for round 1, 100 nM for rounds 2–5, and 33, 3.3, 1.0, 0.33, and 0.10 nM for rounds 6–10, respectively.

To separate protein-bound from -unbound nucleic acids, AF-labeled protein was captured on protein G magnetic beads (Dynabeads) via a rabbit IgG anti-AF Ab (Invitrogen, Molecular Probes), whereas biotinylated protein was captured on MyOne Streptavidin paramagnetic beads (Invitrogen). AF capture beads were prepared by incubating 70 μg of rabbit IgG anti-AF Ab with beads (10 mg) in 1 ml of SB18T0.05 buffer (as described for SB18T0.01 except with 0.05% [v/v] Tween 20). After a 30 min incubation at 37°C, beads were washed three times with 14 ml of SB18T0.05 and stored at 4°C until use. Round 1 was performed using FB preimmobilized on beads, whereas in all other rounds, FB was captured after a binding step in solution. A kinetic challenge consisting of 5 mM dextran sulfate and counter SELEX against capture beads and a protein competitor mixture (10 μM casein, 0.1% [w/v] human serum albumin, and 10 μM prothrombin) was employed in rounds 2–10.

The round 10 enriched pool was amplified by PCR and the products purified by SDS-PAGE. Following buffer exchange, ion torrent sequencing was performed by SeqWright Genomic Services (GE Healthcare, Houston, TX).

Aptamer synthesis

Aptamers were synthesized by standard DNA phosphoramidite methods (32). The phosphoramidites for modified 2NEdU bases were synthesized as described elsewhere (30, 33). For crystallography studies, aptamers were purified using ion-pairing reverse phase liquid chromatography, followed by desalting using Hi-Trap Sephadex G-25 columns (GE Life Sciences). Desalted aptamers were evaporated to dryness using a Genevac HT-12 system. The purified products were characterized by ultra-performance liquid chromatography (Waters ACQUITY System) and their identities confirmed by MALDI-TOF mass spectrometry.

Binding affinity determinations

Equilibrium binding constants (K_d) in solution were measured as described previously (29). Briefly, radiolabeled aptamer [^{32}P] was incubated at 37°C with varying FB concentrations, and complexes were captured after 30 min using Zorbax PSM-300 resin (Agilent Technologies, Santa Clara, CA). Bound aptamer was quantified with a phosphorimager. The percent of maximum captured aptamer was plotted versus the logarithm of protein concentration. These data were then fitted to a four-parameter sigmoid dose-response model to determine the apparent K_d.

Nuclease stability assays

Aptamers (250 nM) were incubated with 0.2 U/ml of recombinant human DNase I (Cell Sciences) in a buffer consisting of 10 mM Tris HCl (pH 7.6), 2.5 mM $MgCl_2$, and 0.5 mM $CaCl_2$ or with 140 U/ml of porcine DNase II (Worthington Biochemical) in a buffer consisting of 0.1 M sodium acetate (pH 4.6), 2.0 mM $MgCl_2$, and 15 mM NaCl. Incubations were conducted at 37°C in a total reaction volume of 100 μl. At the indicated times, a 15 μl aliquot was collected and the reaction stopped by adding an equal volume of 2× gel loading buffer (93.85% [v/v] formamide, 0.2% [w/v] SDS, 20 mM Na_2EDTA, 0.05% [w/v] xylene cyanol, and 0.1% [w/v] Orange G) and heating at 95°C for 2 min. Serum stability studies were performed in 90% (v/v) pooled human sera with 10% (v/v) PBS using a final aptamer concentration of 500 nM. Samples were processed as described by Gupta et al. (34). Briefly, aliquots were extracted with phenol–chloroform and concentrated using a YM-10 m.w. cutoff filter (EMD Millipore). Digestion products for all studies were separated from full-length aptamer by PAGE (15% [w/v] polyacrylamide gel containing 8 M urea) using a Tris–borate buffer system. Electrophoresis was carried out for 20 min at 200 V. Aptamers were stained with 2 μM SYBR Gold nucleic acid stain (Molecular Probes), imaged using a FluorChemQ imager (Alpha Innotech), and quantified using AlphaView Q software with background subtraction. Data are presented as the percentage of full-length input aptamer. All aptamers used in these studies had a 5′-hydroxyl group and 3′–3′-linked dT cap.

Hemolysis assays

AP hemolysis assays were conducted in a 100 μl reaction mixture consisting of 10 μl normal human serum (NHS), 55 μl of 0.1% (w/v) gelatin veronal buffer (GVB; Complement Technologies), 10 μl of 0.1 M MgEGTA (Complement Technologies), 5 μl aptamer in double-distilled H_2O to achieve the indicated final concentration, and 20 μl of rabbit erythrocytes (5×10^8/ml exchanged into GVB). After 30 min at 37°C, samples were centrifuged for 10 min at 200 × *g*, the supernatant was diluted 4-fold in water, and the absorbance was determined at 412 nm. The percentage of lysis inhibition was determined by the following equation: $100 - [100 \times (OD_{412,\ sample} - OD_{412,\ buffer}/(OD_{412,\ no\ inhibitor} - OD_{412,\ buffer})]$, and the IC_{50} was determined by a four-parameter fit. A similar procedure was employed when using 12% (v/v) FB-depleted serum, except that the erythrocytes were at 3.3×10^8/ml, and the GVB concentration was adjusted to allow for the additional serum and for a 5% (v/v) addition of 20 nM FB. CP assays were performed in a 75 μl reaction mixture consisting of 1.5 μl of C5-depleted NHS and 46 μl of GVB containing of 10 mM $MgCl_2$ and 10 mM $CaCl_2$ (GVB^{++}). After addition of human FB (4 μl, 2 nM final concentration) and aptamer (7.5 μl) to achieve the desired concentration, 16 μl of Ab-sensitized sheep erythrocytes (3.3×10^8/ml exchanged into GVB^{++}) were added. After 30 min at 37°C, the samples were processed as described above. ANOVA with a Dunnett posttest correction was performed by comparing all groups to the no inhibitor control.

The aptamers used in this study typically exhibit K_d values for their target protein that are orders of magnitude below the concentrations of the target protein in serum samples. Because of this, any experiment done in dose-response fashion using normal serum would be expected to show an IC_{50}-type value near the concentration of the target protein that is being inhibited following correction for dilution. Thus, to investigate the potency of these aptamers in complex and physiologically relevant mixtures, we occasionally made use of target protein–depleted serum samples that were then fortified with a lower final concentration of the target protein prior to experimentation. This approach was used for the AP hemolysis assays shown in Fig. 2B that were performed with FB-depleted/fortified serum. It was also used for the CP hemolysis assays shown in Fig. 2D that were performed with C5-depleted/fortified serum, as the positive control (ARC1905) is a potent C5 inhibitor.

C3a detection assay

C3a detection assays were performed in a 50 μl reaction mixture containing 5 μl NHS and 40 μl of GVB containing 10 mM MgEGTA. After addition of aptamer in water (2.5 μl) to achieve the desired concentration, reactions were initiated by adding 2.5 μl of preactivated zymosan A (10 mg/ml). Following 30 min at 37°C, zymosan was pelleted by centrifugation (10,000 × *g* for 4 min), and the C3a concentrations in the supernatant were determined by ELISA according to the manufacturer's directions (OptEIA human C3a; BD Biosciences).

Crystallization, x-ray diffraction data collection, and structure determination

Samples of SL1102 or SL1103 bound to FB were prepared by mixing a 1.05-fold molar excess of either aptamer with native FB that had been purified from human serum (Complement Technologies). Each sample was exchanged into 10 mM HEPES (pH 7.5), 50 mM NaCl using 3-kDa molecular mass cutoff ultrafiltration units (Merck Millipore) and concentrated to 5 mg/ml complex as judged by OD_{280} using the theoretical extinction coefficient for an equimolar complex. Plate-like crystals of the SL1102/FB complex were obtained within 3–7 d at 20°C by vapor diffusion of hanging drops prepared by mixing 1 μl of complex with 1 μl of a precipitant solution consisting of 0.1 M HEPES (pH 7.5), 0.2 M ammonium acetate, and 25% (w/v) polyethylene glycol 3350 and equilibrating over 500 μl of precipitant solution. A similar procedure was used to obtain plate-like crystals of the SL1103/FB complex with the exception that 0.1 M Bis-Tris (pH 6.5) was used in the precipitant solution. Diffraction-quality samples were cryopreserved by quickly soaking crystals in their respective

precipitant solutions supplemented with an additional 10% (w/v) polyethylene glycol 3350 prior to flash cooling in liquid N_2.

X-ray diffraction data were collected from radiation of 0.97243 Å wavelength using beamline 22-ID of the Advanced Photon Source at Argonne National Laboratory. Reflections were indexed in the space group $P2_1$, integrated, and scaled using the HKL-2000 package (35). Owing to the higher resolution of its diffraction dataset, the structure of SL1103/FB was solved first. Briefly, PHASER (36), as implemented within the PHENIX software suite (37, 38), was used to perform molecular replacement using the refined coordinates of human FB as a search model [Protein Data Bank (PDB) entry 2OK5 (23)]. Upon placement of two copies of FB, initial electron density maps were calculated using bulk solvent scaling and B factor refinement in PHENIX.REFINE (37, 38). A preliminary model for SL1103 was constructed by initially identifying positions of aptamer-derived phosphate groups in the F_o-F_c map. The SL1103 model was completed by manual rebuilding following the identification of features in the $2F_o$-F_c and F_o-F_c maps consistent with the sequential 2NEdU bases at positions 26 and 27 of the aptamer. Positional and B factor refinement in PHENIX.REFINE (37, 38) were used to iteratively improve the model for both copies of the SL1103/FB complex by employing noncrystallographic symmetry restraints. The structure of SL1102/FB was solved by molecular replacement using the final model of SL1103 and FB [PDB entry 2OK5 (23)] as sequential search models in PHASER (36). Model building and refinement was carried out using equivalent methods to those described for the SL1103/FB complex.

The final model for SL1103/FB consists of two complete copies of each aptamer including the 3′-inverse dT cap (chains B and D), along with two copies of FB (chains A and C). Residues 1–8, 63–65, 218–232, 321–326, and 703–707 were not modeled in chains A and C because of poor electron density. The final model for SL1102/FB differs in the presence of two additional bases found at the 5′- and 3′-ends, respectively, in each chain (chains B and D). However, neither of these chains includes a 3′-inverse dT cap. The composition of the FB chains modeled in the SL1102/FB structure is identical to those in the SL1103/FB structure. A quantitative description of the cell constants, diffraction data quality, and properties of the final model for each complex can be found in Table II.

Competition binding assays

Competition between SL1103 and FB (Complement Technologies) for binding to C3b was investigated using a surface plasmon resonance (SPR)–based approach on a BiaCore T-200 instrument. A NeutrAvidin (Thermo Fisher Scientific)–derivatized CMD200M chip (Xantec Bioanalytics, Dusseldorf, Germany) was prepared by standard amine coupling and used to capture human C3b that had been site-specifically biotinylated at Cys^{1010} via EZ-link Maleimide-PEG_2-Biotin (Thermo Fisher Scientific) according to previously published protocols (19, 20, 39). A reference surface was prepared by injecting one flow cell (fc) with biotin alone (10 μM) to yield a final capture level of 87 resonance units (RU) (fc1). Replicate experimental surfaces containing 2583 (fc2), 2485 (fc3), and 2685 (fc4) RU of C3b biotin were prepared thereafter by injecting dilute solutions of C3b biotin (8 ng/μl) across the remaining fc.

All binding studies were carried out at 25°C using a running buffer of 20 mM HEPES (pH 7.4), 150 mM NaCl, 0.005% (v/v) Tween 20, and 10 mM $MgCl_2$ and a flow rate of 30 μl/min. Binding of FB to C3b was assessed by injecting a buffer blank, followed by a 2-fold dilution series of FB across eight different concentrations spanning 15.625 nM to 2 μM. Each injection cycle consisted of a 1 min association phase, a 2 min dissociation phase, and final 0.5 min phase in which a solution of 2 M NaCl was used to regenerate the surface. Each reference-subtracted sensorgram series was analyzed using BiaCore T-200 Evaluation software. Data were fitted to a two-state reaction model that incorporates a single second-order association rate constant in which $k_{a,1} = 7.7 \times 10^5\ M^{-1}s^{-1}$, $k_{d,1} = 2.0\ s^{-1}$, $k_{a,2} = 2.9 \times 10^{-3}\ s^{-1}$, $k_{d,2} = 3.9 \times 10^{-3}\ s^{-1}$, and $K_d = 1.4$ μM. Competition binding studies were conducted by including SL1103 at the desired concentration ratio relative to 2 μM FB and injecting the resulting analyte mixture as outlined above. Analysis of these sensorgram series was carried out as described above. Data were normalized by assigning a value of 100% to the signal resulting from injection of the competitor-free, 2 μM FB sample immediately prior to the end of the association phase. Each experimental fc was normalized independently to account for the slight differences in C3b density. All plots were generated using GraphPad Prism v6.07.

Convertase formation assay

FB (Quidel) alone or with SL1102 was prepared at twice the indicated final concentrations in GVB containing 10 mM MgEGTA, and the mixtures were incubated at room temperature for 15 min. An equal volume of the same buffer containing twice the indicated concentration of C3b and FD (Quidel) was added, and the mixture was incubated at 37°C for 30 min. Proteins were then labeled with Alexa Fluor 647 according to the manufacturer's directions (Molecular Probes) and reactions stopped by the addition of 2× Tris–glycine loading buffer. Reactions without SL1102, or without one or more of the protein components, were run in parallel. Proteins were resolved by SDS-PAGE (4–20% (w/v) Tris–glycine; Novex) at 150 V for 1.5 h. The gel was imaged at 632 nm using an AlphaImager.

Miscellaneous

Calculation of buried surface areas and identification of potential polar interactions such as hydrogen bonds were performed using EBI-PISA server (40). LigPlot was also used to illustrate features of surface complementarity and packing interactions (41). Structural superpositions and renderings of molecular structures and surfaces were generated by PyMol (http://www.pymol.org/).

Reference protein sequences were obtained from the National Center for Biotechnology Information (http://ncbi.nlm.nih.gov/) and aligned using BLASTP. The RefSeq accession numbers for FB are NP_001701.2 (*Homo sapiens*), NP_001009169.1 (*Pan troglodytes*), XP_005553497.1 (*Macaca fascicularis*), XP_001113553.2 (*M. mulatta*), XP_003431724.1 (*Canis lupus*), NP_001035616.1 (*Bos taurus*), NP_032224.2 (*Mus musculus*), and NP_997631.2 (*Rattus norvegicus*), whereas the number for C2 (*H. sapiens*) is NP_000054.2.

Results

Identification and characterization of FB-binding, chemically modified aptamers

We screened for aptamers that bind human FB via 10 rounds of the SELEX process using FB isolated from human serum and a DNA library containing a 40-nt random region wherein 2NEdU was uniformly substituted for dT (Fig. 1A). Upon sequencing the enriched pool, we identified a family of sequence-related molecules that contained a 23-nt consensus sequence that accounted for ∼6% of the enriched library (Table I). A single-nucleotide insertion between positions 13 and 14 of the consensus was found in a minority of the sequences we obtained, including the most abundant sequence of the enriched SOMAmer pool. We truncated this most abundant sequence to a 31-mer (SL1100) and to a 29-mer (SL1101), both of which were synthesized with a 3′–3′-linked dT cap to enhance resistance to exonucleases (n.b., that SOMAmer reagent lengths do not include this cap residue). We found that both truncated aptamers maintained high-affinity binding to FB in this configuration with a mean (95% confidence interval [CI]) equilibrium dissociation constant (K_d) of 12 (6.2–17) pM for SL1100 and 12 (6.5–17) pM for SL1101 (Fig. 1B).

We used single dT substitution scans in the context of SL1100 to determine which of the seven 2NEdU nucleotides were most critical to function of this SOMAmer family. Although FB-binding studies showed that all seven modified nucleotides are important to some degree, we observed a clear distinction between substitutions for the three 2NEdU residues closest to the 5′-terminus when compared with the remaining four (Fig. 1C). Whereas single dT substitutions within the first group reduced the affinities by ∼3–6-fold, corresponding substitutions within the second group reduced the affinities from 100- to >10,000-fold (Fig. 1C). This strongly suggested that the bases near the 3′ region of the aptamers might contribute directly to the FB-binding site.

We also carried out a separate substitution scan wherein a 3-carbon alkyl linker (C3 spacer) was incorporated for each base aside from those occupied by 2NEdU (Fig. 1C). This substitution preserves the natural spacing of the aptamer chain, does not impact folding, and therefore allows the functional contributions for each nucleoside base to be determined (34). We found that all C3-spacer substitutions within the consensus sequence of the 29-mer, SL1101, reduced affinity for FB, although the magnitude of the

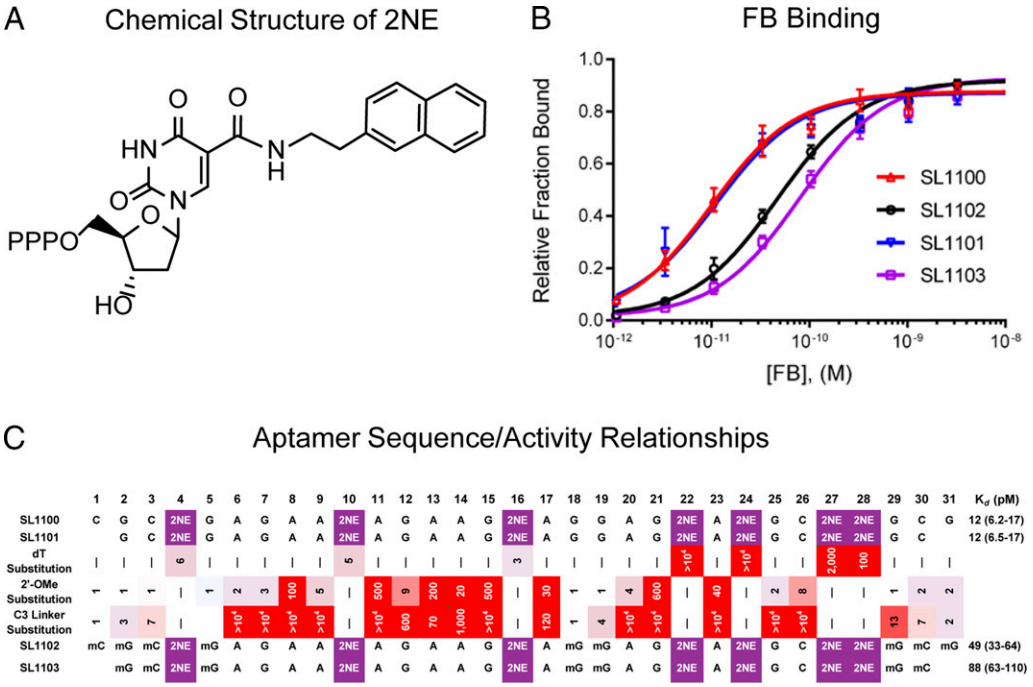

FIGURE 1. Sequence–function relationships of FB-binding SOMAmer reagents. (**A**) Structure of 2NEdU used to uniformly substitute for dT in the SELEX library. The triphosphate is indicated as PPP. (**B**) Binding curves of aptamers as shown in (**C**). Symbols represent mean (SEM) percent maximum binding for seven, four, eleven, and eight independent determinations for SL1100, SL1101, SL1102, and SL1103, respectively. Data were fitted to a four-parameter sigmoid dose-response model to determine the apparent equilibrium dissociation constants (K_d) for each interaction. (C) Sequence–function relationships and post-SELEX modification of the truncated aptamer, SL1100. Results of dT, C3 (3-carbon alkyl linker in place of the nucleoside), and 2′-OMe substitution scans are shown as the affinity ratio (K_d variant/K_d parent) for each single substitution. The effect on binding is also indicated by color, with affinity loss being red where color intensity is related to the magnitude of the change. A vertical dash (|) indicates that no affinity data were acquired. Sequences of SL1100, SL1101, and the 2′-OMe–substituted aptamers SL1102 and SL1103 are shown where the position of a 2′-OMe sugar is indicated with the letter m preceding the nucleobase designation. Equilibrium dissociation constants are given as the mean along with the CIs (95% CI).

loss was <10-fold for those bases at and proximal to the 5′ and 3′ termini. Interestingly, we also determined that the guanosine at position 18 could be replaced with a C3 spacer without loss of binding affinity, as was suggested by the family of sequences obtained from the initial enriched library (Table I). In fact, deletion of this nucleoside entirely had no impact on FB-binding affinity of the SOMAmer (data not shown).

DNA aptamers with modified nucleosides have been shown to possess increased resistance to nucleases in serum when compared with native DNA of the same sequence (34, 42). Consistent with these observations, we found that in vitro stability of SL1100 against 90% (v/v) NHS, 0.2 U/ml human rDNase I, or 14 U/ml porcine DNase II was increased by 14-, 17-, and 6-fold, respectively, when compared with a version of SL1100 in which all seven 2NEdU residues were replaced with natural dT residues (Supplemental Fig. 1). To further enhance nuclease resistance, we substituted 2′-*O*-methyl ribose (2′-OMe) for 2′-deoxyribose sugars where permitted. Positions that could tolerate a 2′-OMe group were determined by substitution scanning of SL1100 and resulted in the creation of aptamers containing nine and seven 2′-OMe residues for the 31-mer (SL1102) and 29-mer (SL1103), respectively (Fig. 1C). This process increased the nuclease resistance of SL1102 by 3.4-fold against DNase I and 4-fold against DNase II. We also found that both SL1102 and SL1103 were completely stable for 96 h at 37°C in 90% (v/v) pooled NHS (Supplemental Fig. 1). However, we also noted that these 2′-OMe substitutions resulted in slight reductions in binding affinity (Fig. 1B). The mean (95% CI) K_d for SL1102 was 49 (33–64) pM, which represented a 4-fold reduction from its parent molecule SL1100. Similarly, the mean (95% CI) K_d for SL1103 was 88 (63–110) pM, which equated to a 7.3-fold reduction from its parent molecule SL1101.

FB-binding SOMAmers inhibit the AP of complement

Although our initial studies demonstrated that this novel family of SOMAmer reagents bound FB with high affinity, they did not determine whether these molecules had any effect on FB activity. We therefore examined the outcome of including these aptamers in various assays for complement function. We initially tested the ability of each aptamer to inhibit lysis of rabbit erythrocytes using 10% (v/v) NHS as a source of complement components and conditions specific for the AP (please see *Materials and Methods*). Significantly, we found that SL1100, SL1102, and SL1103 each inhibited lysis in a dose-dependent manner with IC_{50} values of 220, 200, and 280 nM, respectively (Fig. 2A). FB is present at concentrations of ~200 μg/ml in human plasma, which corresponds to ~2 μM protein. As this value is greater than five orders of magnitude above the K_d of these SOMAmer reagents for FB (Fig. 1B), we repeated the rabbit erythrocyte lysis assay using 12% (v/v) FB-depleted NHS that had been fortified with 20 nM FB. Under these conditions, we found that SL1102 inhibited lysis with an IC_{50} value of 9.8 nM (Fig. 2B). This suggested that the apparently weaker potency of the aptamers in our initial experiment was due to the large quantities of FB present in NHS rather than a change in their ability to bind to FB in complex mixtures.

Because FB is required for forming the AP C3 convertase, any inhibitors of FB activity should also disrupt C3 activation under conditions specific for the AP. To test this hypothesis for the FB-binding aptamers, we included varying concentrations of SL1100

Table I. Sequence distribution of FB-binding aptamers

Identical Copies	Equivalent Copies	Total	Sequence 5′→3′[a]
189	429	618	5′-GACACGCt**GAGAAtAGAAGtAGGAGtAtGCtt**GCGACCAC-3′
113	71	184	5′-t**GAGAAtAGAAGtA-GAGtAtGCtt**AAGtAGGGCGtCAGtC-3′
98	87	185	5′-tCtGACCGAt**GAGAAtAGAAGtA-GAGtAtGCtt**CGGtGGC-3′
79	38	117	5′-AAtCCCt**GAGAAtAGAAGtAtGAGtAtGCtt**GGGtGGGA-3′
25	104	129	5′-AAGttGACACG**GAGAAtAGAAGtA-GAGtAtGCtt**AGAtGt-3′
17	23	40	5′-A**GAGAAtAGAAGtA-GAGtAtGCtt**GAGGttAtGGtCACGt-3′
15	22	37	5′-GCtGGCAt**GAGAAtAGAAGtAGGAGtAtGCtt**GAACAGAC-3′
10	27	37	5′-tGCA**GAGAAtAGAAGtA-GAGtAtGCtt**GCACCtAACAAGG-3′
9	13	22	5′-CG**GAGAAtAGAAGtA-GAGtAtGCtt**AGCAGtGAAGGCtCCAGA-3′
6	3	9	5′-AACttAAGCAt**GAGAAtAGAAGtA-GAGtAtGCtt**GCGtAC-3′
5	6	11	5′-GGtGCtGAAAAAtGCC**AGAAtAGAAGtA-GAGtAtGCtt**GG-3′
5	4	9	5′-A**GAGAAtAGAAGtA-GAGtAtGCtt**AAAGGAtGtAtCGGCt-3′
3	3	6	5′-CCACAAtAGCCGt**GAGAAtAGAAGtACGAGtAtGCtt**GGCtCC-3′
3	0	3	5′-CtttGGCGCG**GAGAAtAGAAGtA-GAGtAtGCtt**AGCtCCA-3′
3	0	3	5′-CtACtGtGCA**GAGAAtAGAAGtA-GAGtAtGCtt**GCACCtAACAAGG-3′
2	2	4	5′-t**GAGAAtAGAAGtA-GAGtAtGCtt**AAGAAAtGGGGAGAtG-3′
2	1	3	5′-ttGGCt**GAGAAtAGAAGtAGGAGtAtGCtt**GCCtGGGCAC-3′
2	1	3	5′-**GAGAAtAGAAGtA-GAGtAtGCtt**AGGtAtGAAGGCtCCAGG-3′[b]
2	0	2	5′-**GAGAAtAGAAGtA-GAGtAtGCtt**AGGttGGGGCtACCAtCA-3′[b]
2	0	2	5′-A**GAGAAtAGAAGtA-GAGtAtGCtt**CAAGGCAGAGCAGGGCA-3′
2	0	2	5′-GtGAAGCAGt**GAGAAtAGAAGtA-GAGtAtGCtt**AAGCGGt-3′

[a]The sequences in bold represent the consensus obtained following SELEX.
[b]The first G occurred as part of the fixed region of the 5′ primer.

and SL1102 in an assay in which zymosan A was used to stimulate the complement activity of 10% (v/v) NHS in the presence of MgEGTA and then measured the levels of C3a that resulted. We observed dose-dependent inhibition of C3 activation by SL1100 and SL1102 with IC_{50} values well matched to the concentration of FB, as judged by an ELISA specific for C3a (Fig. 2C). As a control for specificity, we tested whether the same aptamers could inhibit lysis of Ab-sensitized sheep erythrocytes in the presence of 2% (v/v) C5-depleted serum that had been fortified with 2 nM C5.

We found that including 2 μM of the C5-targeted aptamer ARC1905 (43) completely inhibited hemolysis, but neither SL1100 nor SL1102 had any impact on hemolysis when used at the same concentration (Fig. 2D). Thus, this family of FB-binding SOMAmers act as specific inhibitors of the complement AP.

SL1102 and SL1103 bind FB at the juncture of its CCP1, CCP3, and vWF domains

We sought structural information to better understand the physical basis for inhibition of the AP by these FB-binding SOMAmer reagents. To that end, we crystallized SL1102 and SL1103 bound to human FB, collected x-ray diffraction data, and solved each structure by molecular replacement using a structure of FB as an initial search model (23). Because the diffraction data for the SL1103/FB crystal extended to 3.1 Å, limiting resolution, whereas that from the SL1102/FB crystal extended to only 3.5 Å (Table II), we completed the SL1103/FB structure first then used the refined model for SL1103 (29 bases) as starting model for SL1102 (31 bases). The final models for SL1103/FB and SL1102/FB had R_{work} and R_{free} values of 20.8/24.1 and 22.7/25.7%, respectively (Table II). Each model contains two copies of the aptamer/FB complex in the asymmetric unit that are related by noncrystallographic symmetry (Supplemental Fig. 2). Aside from the presence of an additional base pair formed by extension of the 5′ and 3′ ends in SL1102 when compared with SL1103 (Supplemental Fig. 2, Table I), the individual aptamer/FB complexes are practically indistinguishable from one another as judged by structural superposition (data not shown). Consequently, we restricted subsequent analyses to the complex represented by chains A and B in the SL1103/FB structure.

The SL1103 molecule adopts a compact, cylinder-like fold that is ~50 Å in length and 20 Å in diameter. SL1103 resembles a spiral staircase when viewed as a ribbon diagram in which the railing is comprised of the aptamer sugar–phosphate backbone (Supplemental Fig. 3A). Position mG-17 in SL1103 (mG-18 per the numbering convention used in Fig. 1C) represents the second pivot point in this SL1103 staircase (Supplemental Fig. 3A); its guanine base does not pack within the core of the SOMAmer but instead is solvent exposed. Not surprisingly, mG-17 is the only nonterminal position permissive of substitution with a C3 spacer (Fig. 1C), as this base may be deleted without compromising binding. Aside from this, the core of the SL1103 molecule is held together by extensive base-stacking and base-pairing interactions (Supplemental Fig. 2C). The most noteworthy of these are a series of triplex-like structures formed by coplanar arrangements of C-25, G-6, and G-14 as well as A5 and the uracil-like moieties of 2NEdU-26 and 2NEdU-15 (Supplemental Fig. 3B). The existence of these unconventional interactions is supported by appropriate hydrogen bond distances (i.e., 2.7–3.4 Å), unambiguous $2F_o$-F_c electron density at reasonably high contour levels (e.g., 1.3σ), and strong model-to-map correlations in these areas (Supplemental Fig. 2C, 2D).

The seven modified 2NEdU bases also feature prominently in the SL1103 structure (Supplemental Fig. 3C). The first cluster of four 2NEdU is found near the middle of the SL1103 molecule and is comprised of positions 3, 15, 26, and 27. In an earlier experiment, we determined that dT substitution at positions 3 and 15 had relatively mild effects on aptamer function, but loss of the 2NEdU at positions 26 and 27 essentially abolished inhibitory activity (Fig. 1C). Consistent with these observations, the 2NEdU sidechains from positions 26 and 27 appear to participate in base-stacking interactions in the middle of the aptamer that may be required for proper folding of the nucleic acid chain (Supplemental Fig. 3D). The second cluster of three 2NEdU is comprised of positions 9, 21, and 23 and lies at the end of the aptamer structure opposite the 5′ and 3′ termini. Interestingly, we also found in an earlier experiment that substitution of positions 21 and 23 by dT abolished aptamer function (Fig. 1C). Although it is unclear if these positions are required for structural stability of the aptamer molecule, they

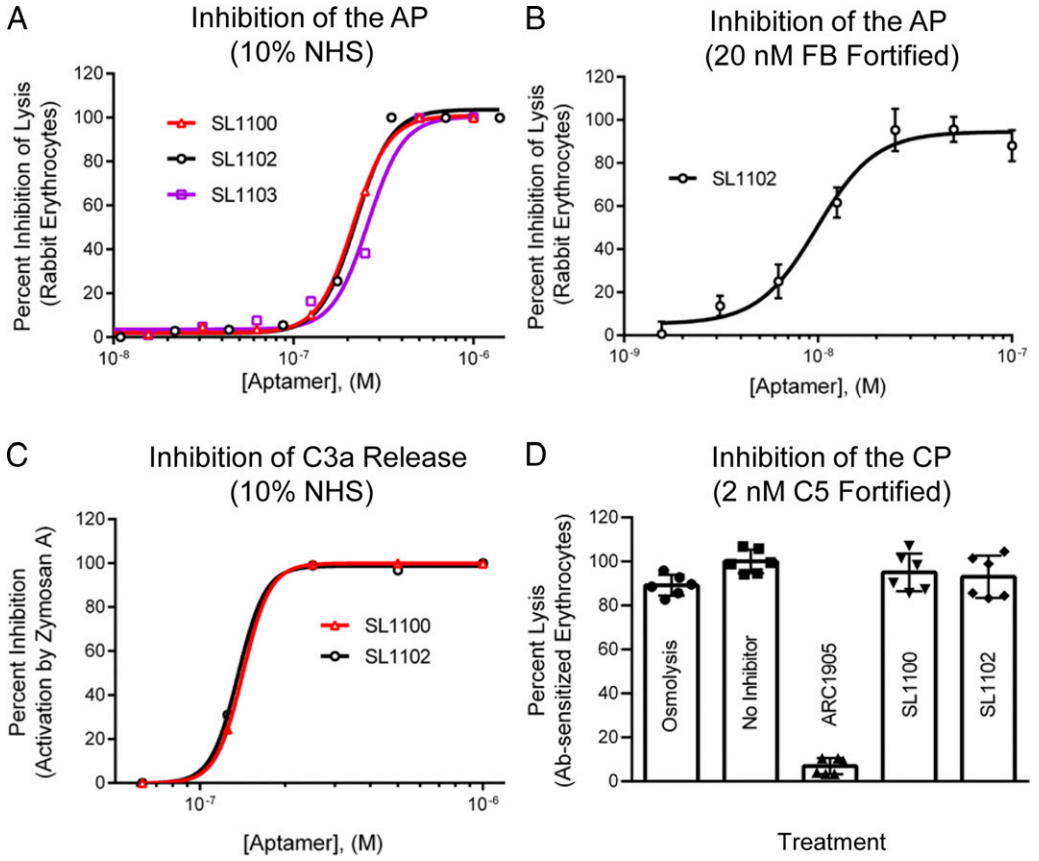

FIGURE 2. FB-binding SOMAmer reagents inhibit the AP, but not the CP of complement. (**A**) FB-binding SOMAmer reagents inhibit hemolysis of rabbit erythrocytes in the presence of 10% (v/v) NHS. The IC_{50} values for SL1100, SL1102, and SL1103 are 220, 200, and 280 nM, respectively. (**B**) SL1102 inhibits hemolysis of rabbit erythrocytes in the presence of 12% (v/v) FB-depleted NHS fortified with 20 nM of human FB. The mean ± SD of the percent lysis observed in three independent determinations is shown (IC_{50} = 9.8 nM). (**C**) FB-binding SOMAmer reagents inhibit generation of C3a in 10% (v/v) NHS stimulated with zymosan A. Both SL1100 and SL1102 blocked activation of C3 in a dose-dependent manner. (**D**) FB-binding SOMAmer reagents do not inhibit the CP of complement. The percent lysis of Ab-sensitized (Ab-sensitized) sheep erythrocytes in 2% (v/v) C5-depleted NHS fortified with 2 nM human C5 is shown as the mean ± SD of six independent determinations. No significant difference in hemolysis was observed with the addition of either 2 μM SL1100 ($p = 0.52$) or SL1102 ($p = 0.25$) when compared with the no inhibitor control. The anti-C5 aptamer, ARC1905 (40 nM), served as a positive control and inhibited hemolysis ($p < 0.001$).

do form a knot-like structure that contributes significantly to the FB-binding surface of SL1103, as described below.

SL1103 binds FB at groove-like surface lying at the juncture of the CCP1 and CCP3 domains from Ba and the vWF domain from Bb (Fig. 3A, Supplemental Fig. 2E, 2F). Approximately half of the buried surface area in the SL1103-binding site is derived from the CCP1 domain, with the remainder equally portioned from the CCP3 and vWF domains. CCP1 also participates in 12 of the 16 intermolecular hydrogen bonds found in the SL1103/FB complex. Together, these lines of evidence suggest that CCP1 is the primary recognition site for SL1103. Within SL1103, the FB-binding site assembles from two sets of noncontiguous bases (Fig. 3B, Supplemental Fig. 3E, 3F) that are found in proximity to one another in the folded aptamer (Fig. 3C). The first of these (site 1) is comprised of positions 8 through 11 and includes a single 2NEdU modification at position 9. Site 1 accounts for ~454 $Å^2$ of buried surface area from SL1103 and appears to form 10 hydrogen bonds with groups found within CCP1 of FB (Fig. 3D, Supplemental Fig. 3E, 3F). Five of these hydrogen bonds involve atoms from the sugar–phosphate backbone of 2NEdU-9. The second site (site 2) is comprised of positions 21 through 24 and includes two 2NEdU modifications at positions 21 and 23. Site 2 accounts for ~637 $Å^2$ of buried surface area from SL1103 and appears to form six hydrogen bonds with groups found within the CCP1, CCP3, and vWF domains of FB (Fig. 3E, Supplemental Fig. 3E, 3F). The defining features of site 2 include three hydrogen bonds between the adenine base of A-22 and Thr^{48} and Ser^{196} of FB, as well as extensive packing interactions between these positions and nearby surfaces derived from FB (Fig. 3F). It is interesting to note that the sidechain modifications of 2NEdU-21 and -23 adopt conformations whereby their naphthyl groups are nearly stacked upon one another and form a platform to display the adenine base from position 22, which forms three hydrogen bonds with FB. This peculiar structural arrangement resembles a molecular knot and is difficult to envisage absent the 2NEdU modifications (Fig. 3E, 3F). Indeed, our previous experiments showed that dT or C3-spacer substitution at any of these positions abolished function and argue for an essential role for site 2 in aptamer activity (Fig. 1C).

FB-binding aptamers inhibit the AP by blocking formation of the Pro-C3 convertase

Whereas biochemical studies of FB binding to C3b have revealed two mechanistically distinct steps that are dependent on Ba and Bb, respectively (17, 22, 24, 25), the physical basis for these interactions is most readily appreciated by examining the crystal structure of FB bound to C3b (25) (Fig. 4A). In this regard, this structure of the so-called Pro-C3 convertase shows that CCP1 of the Ba fragment and the vWF domain of the Bb fragment each from close associations with the C345c domain of C3b (Fig. 4B). Given the location of the aptamer binding site at the juncture of

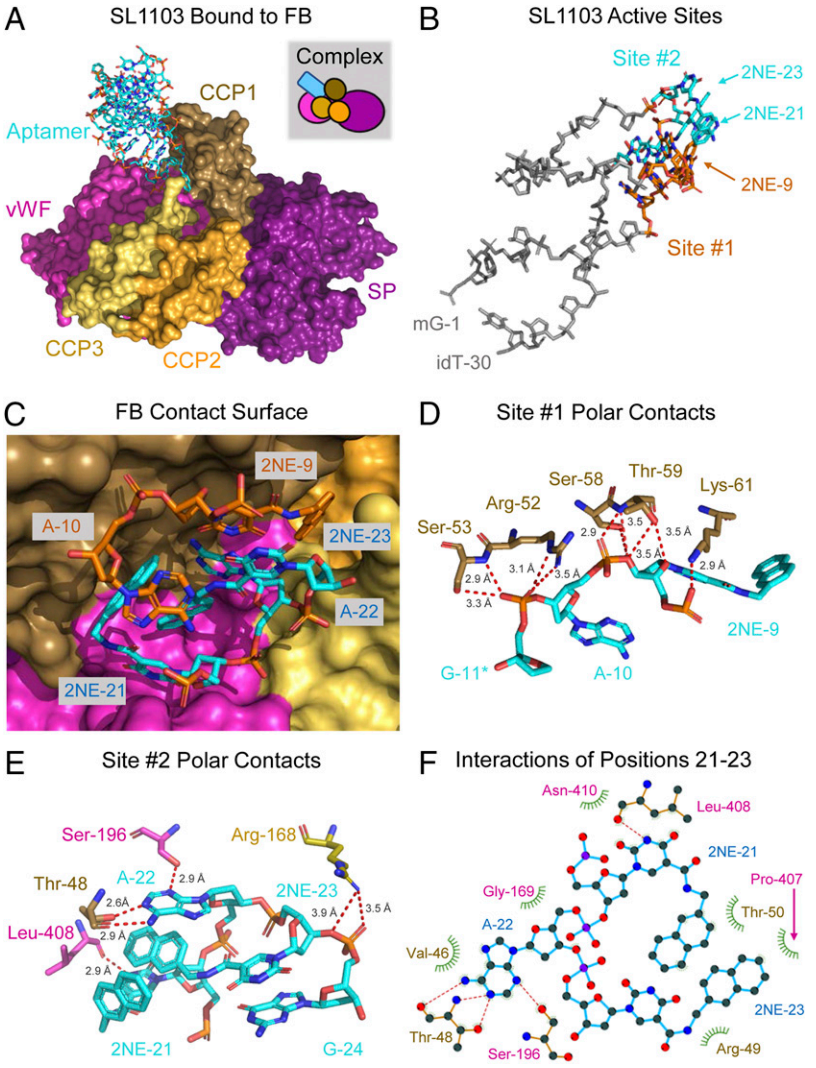

FIGURE 3. Structural analysis of SL1103 bound to FB. (**A**) Structure of the SL1103/FB complex at 3.1 Å limiting resolution, as represented by chains A and B in the PDB deposition 7JTN. SL1103 is drawn in ball-and-stick convention with carbon atoms in cyan, oxygen atoms in red, and phosphorous atoms in orange. FB is depicted as a molecular surface in which each domain is colored differently. A cartoon representation of the complex is shown in the gray box, similarly to Supplemental Fig. 2. (**B**) Location of the FB-binding sites in SL1103. The aptamer is drawn in ball-and-stick convention in which the sugar–phosphate atoms of the backbone are shown for all residues, whereas the nitrogenous bases are also shown for FB-binding site 1 (carbon atoms in orange) and site 2 (carbon atoms in cyan). The locations of selected positions in SL1103 are indicated. (**C**) Closeup representation of the FB contact surface in SL1103. FB is depicted identically to (A), whereas the positions from FB-binding site 1 (carbon atoms in orange) and site 2 (carbon atoms in cyan) are shown in ball-and-stick convention. (**D**) Polar contacts in FB-binding site 1 of SL1103. Residues in FB are shown in ball-and-stick convention with the same coloring scheme as (A), whereas positions from SL1103 are shown with carbon atoms colored cyan. Likely hydrogen bonds are represented by red dashes, along with their respective distances in angstroms. Note that the nitrogenous base of G-11 is hidden for the sake of clarity. (**E**) Polar contacts in FB-binding site 2 of SL1103. Representations and coloring schemes are identical to those in (D). (**F**) Schematic representation of the packing interactions between FB-binding site 2 of SL1103 and FB. Positions 21–23 of the aptamer are drawn with their carbon atoms in blue, whereas groups from FB are depicted according to the color scheme of (A). Hydrophobic/packing interactions are represented by green arcs, whereas residues that participate in polar interactions are shown in ball-and-stick convention. Likely hydrogen bonds are represented by red dashes.

the CCP1, CCP3, and vWF domains (Fig. 3), we hypothesized that aptamer binding to FB would block FB/C3b binding through the mechanism of steric hindrance (Fig. 4C). Blocking formation of the Pro-C3 convertase in this manner would prevent formation of the active C3 convertase (Fig. 4D) and therefore explain the potent inhibitory effects of these SOMAmer reagents on the AP (Fig. 2).

To test this hypothesis directly, we employed a competition-style assay that was derived from an established SPR method for monitoring FB binding to site-specifically immobilized C3b (17, 19, 25, 44). As expected, we found that injection of increasing concentrations of FB over a C3b surface yielded a strong, dose-dependent binding response that could be fit to a two-step association model (17, 25) (Fig. 5A). However, when we repeated this experiment using analyte solutions that contained increasing concentration ratios of SL1103 in addition to FB, we observed that the FB-binding response decreased dramatically (Fig. 5B–D). We detected no binding at all when equal concentrations of FB and SL1103 were injected over the C3b surface (Fig. 5E). When we examined the SPR response immediately prior to injection stop, we found that increasing concentrations SL1103 resulted in progressively greater inhibition of FB binding across all injection points used (Fig. 5F). Together, these experiments showed that inclusion of SL1103 had the apparent effect of reducing the effective concentration of FB present. Therefore, they demonstrate that these FB-binding SOMAmer reagents inhibit formation of the AP Pro-C3 convertase in a purified setting.

As a final test of the functional consequences of this competitive effect, we examined whether members of this aptamer family could block formation of the active AP C3 convertase (Fig. 6). When we incubated purified FB and C3b at equimolar concentrations then added catalytic quantities of FD, we observed the generation of two species indicative of FB cleavage into its Ba and Bb fragments. However, when we repeated this experiment in the presence of increasing concentrations of SL1102, we observed a dose-dependent decrease in the extent of FB cleavage into Ba and Bb. We also noted that when SL1102 was included at a concentration roughly half that of FB, the level of FB cleavage was likewise roughly half that of the uninhibited reaction. This finding was consistent with the long-standing observation that FD cannot cleave FB unless it is bound to C3b (or a closely related molecule like cobra venom factor) (45). It also ruled out the possibility that aptamer binding might have somehow altered this property and led to consumptive cleavage of FB. Consequently, this experiment demonstrated that FB binding by this family of SOMAmer reagents inhibits formation of the active AP C3 convertase in addition to inhibiting formation of the AP Pro-C3 convertase (Fig. 7).

Discussion

In this report, we have described the identification, structure, and functional characterization of a family of DNA aptamers that bind FB with picomolar affinity and inhibit the complement AP. Unlike

Table II. X-ray diffraction data collection and refinement statistics

	SL1103/FB (7JTN)	SL1102/FB (7JTQ)
Data collection		
Space group	$P\ 2_1$	$P\ 2_1$
Cell dimensions		
a, *b*, *c* (Å)	87.13, 144.41, 87.19	87.04, 145.75, 87.06
α, β, γ (°)	90.00, 109.46, 90.00	90.00, 109.62, 90.00
Resolution (Å)	50.00–3.10 (3.21–3.10)	50.00–3.50 (3.63–3.50)
No. of reflections	36,509 (3525)	24,998 (2428)
Completeness (%)	99.4 (96.0)	97.3 (93.6)
$I/\sigma I$	7.2 (1.4)	4.1 (1.2)
R_{pim}	0.101 (0.461)	0.147 (0.461)
$CC_{1/2}$	0.917 (0.573)	0.931 (0.590)
Redundancy	5.7 (4.1)	3.4 (3.0)
Refinement		
R_{work}/R_{free} (%)	20.8/24.1	22.7/25.7
No. of atoms	12,542	12,610
Protein	11,080	11,098
Aptamer	1462	1512
Ramachandran plot		
Favored/allowed (%)	94.4/5.5	93.0/6.6
B-factors (range and mean)		
Protein	16.86–185.84 (61.18)	32.99–194.27 (82.16)
Aptamer	23.22–172.75 (58.69)	50.29–187.98 (84.46)
Root mean square deviations		
deviations		
Bond lengths (Å)	0.013	0.009
Bond angles (°)	1.62	1.33

Values in parentheses are for the highest-resolution shell.

conventional aptamers, these so-called SOMAmer reagents incorporate chemical modifications of the sugar–phosphate backbone, such as 2′-*O*-methylation and a 3′–3′-inverse dT cap, to improve their stability against degradation by nucleases. They also make use of the unconventional nucleotide, 2NEdU, in place of dT (30). This latter modification imparts unique structural and functional properties to SOMAmer reagents and results in significantly increased affinities for their targets (29, 31). Indeed, the

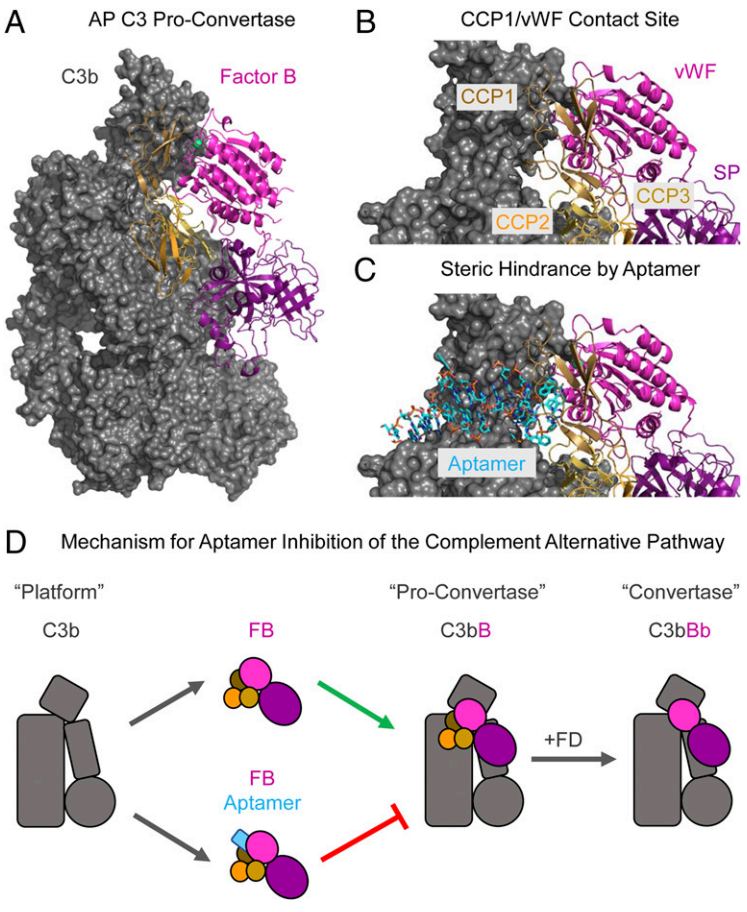

FIGURE 4. Proposed mechanism for AP inhibition by FB-binding SOMAmer reagents. (**A**) Structure of the AP Pro-C3 convertase, as rendered from the PDB entry 2XWJ (25). C3b is depicted as a molecular surface, whereas FB is drawn in cartoon convention according to the color scheme used in Fig. 3. The Ni^{++} ion found at the interface between the vWF domain of FB and the C345c domain of C3b is shown as a green sphere. (**B**) Closeup representation of the FB/C3b complex as drawn in (A). The locations of individual domains within FB are highlighted. (**C**) Identical representation to (B), but also showing SL1103 as inferred from the SL1103/FB crystal structure. By binding tightly to this site on FB, SL1103 would be expected to sterically occlude interaction of FB domains CCP1 and vWF with the C345c domain of C3b. (**D**) Schematic portraying a proposed mechanism for AP inhibition by FB-binding SOMAmer reagents. The top pathway shows the normal sequence of events, where FB binds to C3b to generate the Pro-C3 convertase that can be cleaved by FD to yield to the active C3 convertase (i.e., C3bBb). The bottom pathway shows inhibition of Pro-C3 convertase formation due to the presence of the FB-binding aptamer. This sequence of events would block subsequent formation of the active C3 convertase, thereby resulting in potent inhibition of AP activity.

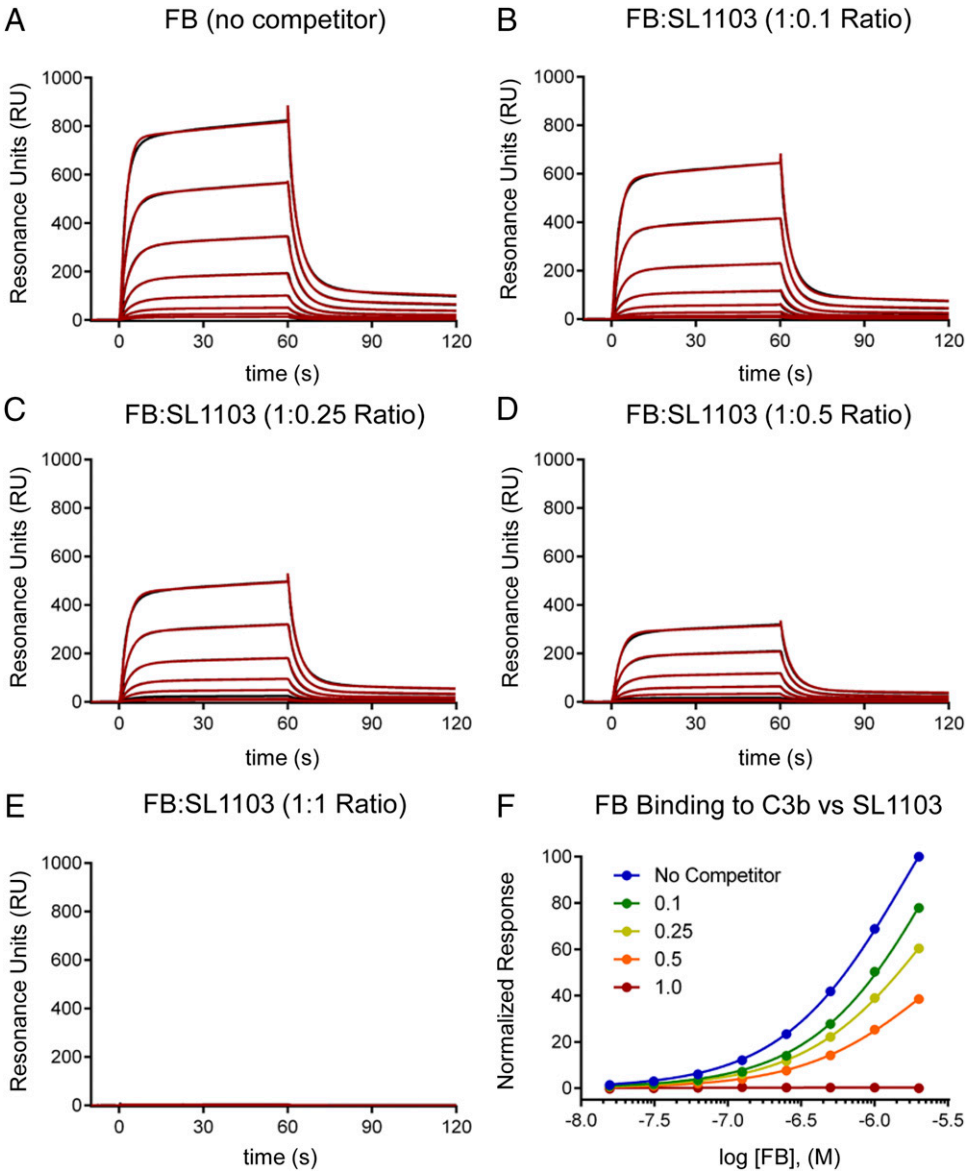

FIGURE 5. FB-binding SOMAmer reagents inhibit formation of the AP Pro-C3 convertase. An SPR sensor surface consisting of site-specifically immobilized C3b was used to investigate binding of FB either alone or in the presence of increasing concentrations of SL1103. A 2-fold dilution series of FB spanning eight different concentrations from 15.625 nM to 2 μM was injected over the surface, and the reference-corrected sensorgrams (black traces) were fit to a two-state reaction model (red traces). (**A**) Binding of FB in the absence of any SL1103. (**B**) Binding of FB in the presence 0.1 M equivalents of SL1103. (**C**) Binding to FB in the presence of 0.25 M equivalents of SL1103. (**D**) Binding of FB in the presence of 0.5 M equivalents of SL1103. (**E**) Binding of FB in the presence of equimolar SL1103. (**F**) Comparison of the normalized SPR response obtained immediately prior to injection stop for each concentration of FB, either in the absence or presence of various levels of SL1103 (legend is inset). Note that increasing levels of SL1103 diminished FB binding to the surface at each FB concentration examined. The data shown represent one of three independent replicates.

FB-binding affinities observed for this chemically modified aptamer family described in this study ranged from 10 to 100 pM (Fig. 1). Subsequent crystal structure determinations for two such SOMAmer reagents (i.e., SL1102 and SL1103) bound to FB revealed that several of the 2NEdU modifications were found at the two contact sites between the macromolecules (Fig. 3, Supplemental Figs. 2, 3) and contributed significantly to the surface area buried at each contact site (Fig. 3, Supplemental Fig. 3). Consequently, these crystal structures confirmed our interpretation of the substitution scanning data, which showed that alteration of the 2NEdU positions essentially abolished the FB-binding properties of the aptamers (Fig. 1). By binding tightly to a site on FB that lies at the juncture of its CCP1, CCP3, and vWF domains (Fig. 4), this family of aptamers prevents FB binding to C3b and subsequent formation the AP C3 convertase (Figs. 5, 6). Ultimately, this results in potent inhibition of the AP (Fig. 2).

The structures of SL1102 and SL1103 in their FB-bound forms share some fundamental features with other complexes of DNA aptamers bound to proteins. For example, SL1103 has a total buried surface area of 1091 $Å^2$ in its target-bound state. This value is comparable to those seen in previous cocrystal structures (i.e., 657–1276 $Å^2$) of DNA aptamers bound to molecules as divergent as thrombin, vWF, and IL-6 (46). Separately, the stacking and clustering of the naphthyl sidechains described in this study for SL1103 has also been observed in the IL-1α–binding SOMAmer reagent, SL1067 (47). Despite these similarities, SL1102 and SL1103 are also defined by features that belie their specificity for FB. These include their ability to form numerous polar interactions with FB as well as what appears to be an

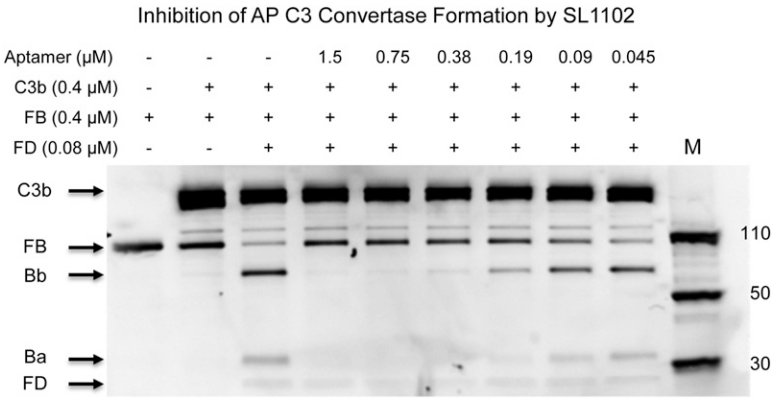

FIGURE 6. FB-binding SOMAmer reagents inhibit formation of the AP C3 convertase. Formation of the AP C3 convertase was monitored by an SDS-PAGE–based method. The appearance of the FB proteolytic cleavage products, Ba and Bb, was only seen when FB is incubated with C3b in the presence of FD. Inclusion of increasing concentrations of the FB-binding aptamer, SL1102, inhibited FB cleavage in a dose-dependent manner, even though all other required components were present. Significantly, convertase formation was blocked at an approximately equimolar ratio between FB and SL1102. Positions of C3b, FB, Bb, Ba, and FD are indicated with arrows. Mass of the protein molecular mass markers (M) are given in kilodaltons. The data shown represent one of three independent replicates.

exceptional level of shape complementary between the SOMAmers and the proprotease (Fig. 3, Supplemental Figs. 2, 3). These attributes were the outcome of a multilayered SELEX process, which used human FB as the target molecule for in vitro evolution of these ligands. Although the family of SOMAmers described in this work binds with picomolar affinity to human FB and potently inhibits human complement, we suspected that the highly optimized nature of their interactions with human FB might also limit the activity of these molecules against FB from more distantly related mammalian species. Indeed, whereas SL1102 blocked hemolysis of rabbit erythrocytes by sera obtained from macaques to essentially the same extent as it did human serum, SL1102 was noticeably less effective in inhibiting hemolysis by rodent sera (Fig. 7A). Given this observation, evaluation of these SOMAmers in various experimental rodent models of complement-mediated diseases might not be appropriate.

To arrive at structural explanation for the functional selectivity of these FB-binding aptamers, we compared the aptamer/FB crystal structures (Fig. 3, Supplemental Fig. 2) to the sequences of FB from various mammalian species along with that of human C2 (Fig. 7B). Although human C2 is the most closely related human protein to FB, roughly three quarters of the C2 residues that correspond to the aptamer binding site of FB were not identical. This very likely explains the failure of SL1100 and SL1102 to inhibit the CP (Fig. 2), presumably because of their inability to bind C2. Moreover, even though FB orthologs from other mammals shared >80% sequence identity to human FB, we still identified several positions within the aptamer binding site that contained substitutions. Most significantly, Thr^{59} in primate FB was changed to Asp and Val in mouse and rat FB, respectively. Although it is worth noting that Thr^{59} forms several backbone- and sidechain-mediated polar interactions with FB-binding site 1 of the aptamers (Fig. 3D), it is unclear at the present time if changes at residue 59 alone could be responsible for the reduced activity against rodent complement. In the future, this limitation might be addressed by reverse-engineering these SOMAmers to gain binding activity toward rodent FB. Alternatively, the SELEX procedure could be redone entirely using rodent FB as the target molecule. Presumably, this would allow identification of analogous families of FB-binding SOMAmer reagents that can inhibit rodent complement with comparable potency. Such work would have the added benefit of allowing for comparisons of inhibition of complement function in different animal models.

Although it was long suspected, work from throughout the last two decades has now firmly established the complement AP as a driving force in many human inflammatory diseases (reviewed in Ref. 3, 5, 6, 48). This has led to considerable interest in developing inhibitors that target the various proteins required for proper

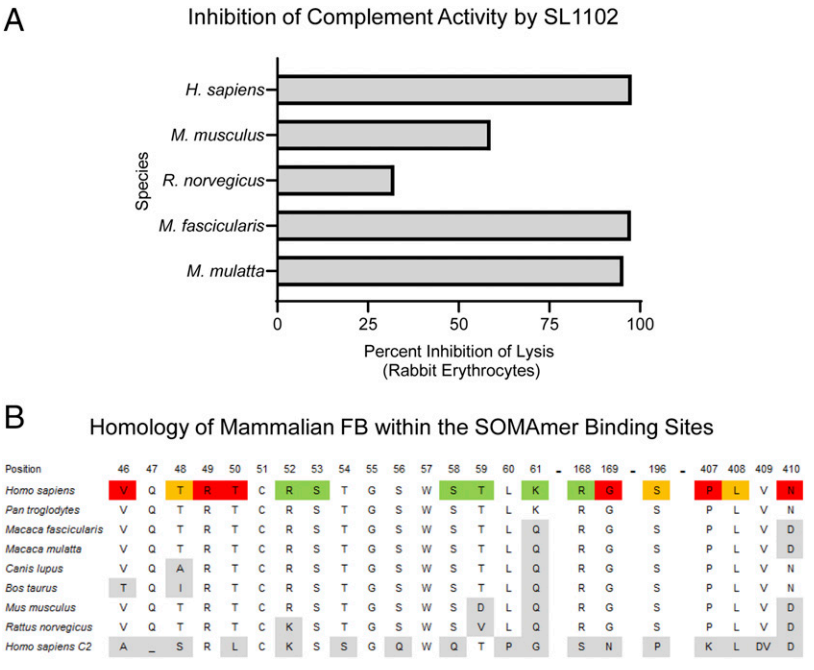

FIGURE 7. Cross-species reactivity of FB-binding SOMAmer reagents. (**A**) Percent inhibition of rabbit erythrocyte hemolysis by 1 μM SL1102 in the presence of 15% (v/v) normal mammalian sera. Note that 2 μM SL1102 and 30% (v/v) mouse serum was used in that experiment only because of its relatively low reactivity. The data shown represent a single determination. (**B**) Homology between the FB proteins from human and representative mammalian species for the amino acids forming major contacts with the FB-binding aptamers. The corresponding sequence for human C2 is shown at the bottom for reference. An underscore symbol represents a deletion in the sequence, whereas the appearance of two residues in a single block represents an insertion. Polar contacts are highlighted in green, those that form packing interactions are highlighted in red, whereas those residues that make both packing and polar contacts are highlighted in orange. Residues that differ from human FB are highlighted in gray. Note that site 1 of the aptamer primarily contacts FB residues 52–61, whereas site 2 contacts FB residues outside that region (see Fig. 3).

AP function as therapeutics (reviewed in Ref. 4, 8). Because the AP C3 convertase is the enzyme underlying the self-amplifying activation of C3 via the AP, it presents perhaps the most attractive target for inhibitor development. Yet the AP C3 convertase itself is comprised of two large molecules in C3b and Bb. It also cleaves one of the most abundant proteins in the blood as its substrate (i.e., C3). These considerations have raised important questions regarding the most effective strategy for blocking convertase activity. In this regard, various mAbs (15, 49), peptidomimetics (8, 50), and even small-molecule inhibitors (39) of C3/C3b function have been described. Several compstatin-class peptidomimetics are now in clinical trials for indications such as periodontal disease, paroxysmal nocturnal hemoglobinuria, and C3 glomerulopathy (8). Nevertheless, targeting FB remains an equally intriguing and complementary approach. To that end, a small-molecule FB inhibitor that appears to reversibly bind the Bb active site and inhibit its enzymatic activity has recently been described (51). This molecule, known as LNP023, has been investigated in rodent models of arthritis and membranous nephropathy and is currently in clinical trials for treatment of paroxysmal nocturnal hemoglobinuria and C3 glomerulopathy (51). Other inhibitors, including two separate FB-binding mAbs, have also been reported and successfully investigated in various disease models (52, 53). These molecules block the AP by inhibiting proconvertase formation, which is also a defining characteristic of the FB-binding aptamers described in this study (Fig. 5). Although none of these inhibitors have progressed to clinical trials, we believe further investigation is warranted, as each of them interferes with an event farther upstream in the AP than does LNP023.

The high-affinity and conformational selectivity with which Abs recognize their targets make them valuable assets for therapeutic manipulation of physiological systems. Although aptamers and related molecules do not possess any of the downstream effector functions of Abs (e.g., opsonization, triggering the CP, etc.), they maintain the ability to bind their cognate ligands with high affinity and potency in a much smaller package (e.g., ~10 kDa). In addition to this, chemical modifications of the sugar–phosphate backbone (e.g., 2′-*O*-methylation) and the inclusion of nonstandard nitrogenous bases provide chemically modified aptamers with significant improvements in nuclease sensitivity and serum stability (Supplemental Fig. 1). This enhanced pharmacological profile, along with their low-cost of synthesis compared with production of proteins like Abs, raises the possibility that they could be powerful tools for inhibiting serum-resident or otherwise extracellular proteins. The generalizable nature of the SELEX process has already enabled identification of SOMAmer reagents that bind over 5000 different human proteins (54). Many of these SOMAmer reagents could be potent inhibitors of complex biochemical networks (e.g., complement, coagulation, etc.) or various signaling axes that control cellular responses (e.g., cytokines, chemokines, etc.). Consequently, SOMAmer reagents and related molecules seem poised to find further applications in the treatment of human disease.

Acknowledgments

We thank Kasra Ramyar, Bret Freudenthal, Amy Gelinas, and Nebojsa Janjic for helpful discussions throughout the course of this work. We also thank Jeff Carter and Matt Otis for the synthesis and purification of SOMAmer reagents. X-ray diffraction data were collected at Southeast Regional Collaborative Access Team 22-ID beamline at the Advanced Photon Source, Argonne National Laboratory. A list of supporting institutions may be found at https://www.ser.aps.anl.gov/. Use of the Advanced Photon Source was supported by the U.S. Department of Energy, Office of Science, Office of Basic Energy Sciences, under contract no. W-31-109-Eng-38.

Disclosures

C.Z. and D.W.D. are employees and shareholders of SomaLogic, Inc. The other authors have no financial conflicts of interest.

References

1. Hajishengallis, G., E. S. Reis, D. C. Mastellos, D. Ricklin, and J. D. Lambris. 2017. Novel mechanisms and functions of complement. *Nat. Immunol.* 18: 1288–1298.
2. Ricklin, D., G. Hajishengallis, K. Yang, and J. D. Lambris. 2010. Complement: a key system for immune surveillance and homeostasis. *Nat. Immunol.* 11: 785–797.
3. Ricklin, D., E. S. Reis, and J. D. Lambris. 2016. Complement in disease: a defence system turning offensive. *Nat. Rev. Nephrol.* 12: 383–401.
4. Ricklin, D., and J. D. Lambris. 2013. Complement in immune and inflammatory disorders: therapeutic interventions. *J. Immunol.* 190: 3839–3847.
5. Ricklin, D., and J. D. Lambris. 2013. Complement in immune and inflammatory disorders: pathophysiological mechanisms. *J. Immunol.* 190: 3831–3838.
6. Reis, E. S., D. C. Mastellos, D. Ricklin, A. Mantovani, and J. D. Lambris. 2018. Complement in cancer: untangling an intricate relationship. *Nat. Rev. Immunol.* 18: 5–18.
7. Morgan, B. P. 2018. Complement in the pathogenesis of Alzheimer's disease. [Published erratum appears in 2018 *Semin. Immunopathol.* 40: 517.] *Semin. Immunopathol.* 40: 113–124.
8. Mastellos, D. C., D. Ricklin, and J. D. Lambris. 2019. Clinical promise of next-generation complement therapeutics. *Nat. Rev. Drug Discov.* 18: 707–729.
9. Rawal, N., and M. K. Pangburn. 2003. Formation of high affinity C5 convertase of the classical pathway of complement. *J. Biol. Chem.* 278: 38476–38483.
10. Rawal, N., and M. Pangburn. 2001. Formation of high-affinity C5 convertases of the alternative pathway of complement. *J. Immunol.* 166: 2635–2642.
11. Harboe, M., G. Ulvund, L. Vien, M. Fung, and T. E. Mollnes. 2004. The quantitative role of alternative pathway amplification in classical pathway induced terminal complement activation. *Clin. Exp. Immunol.* 138: 439–446.
12. Fromell, K., A. Adler, A. Åman, V. A. Manivel, S. Huang, C. Dührkop, K. Sandholm, K. N. Ekdahl, and B. Nilsson. 2020. Assessment of the role of $C3(H_2O)$ in the alternative pathway. *Front. Immunol.* 11: 530.
13. Ricklin, D., E. S. Reis, D. C. Mastellos, P. Gros, and J. D. Lambris. 2016. Complement component C3 - the "Swiss Army Knife" of innate immunity and host defense. *Immunol. Rev.* 274: 33–58.
14. Ferreira, V. P., M. K. Pangburn, and C. Cortés. 2010. Complement control protein factor H: the good, the bad, and the inadequate. *Mol. Immunol.* 47: 2187–2197.
15. Paixão-Cavalcante, D., E. Torreira, M. A. Lindorfer, S. Rodriguez de Cordoba, B. P. Morgan, R. P. Taylor, O. Llorca, and C. L. Harris. 2014. A humanized antibody that regulates the alternative pathway convertase: potential for therapy of renal disease associated with nephritic factors. *J. Immunol.* 192: 4844–4851.
16. Hammel, M., G. Sfyroera, D. Ricklin, P. Magotti, J. D. Lambris, and B. V. Geisbrecht. 2007. A structural basis for complement inhibition by *Staphylococcus aureus*. *Nat. Immunol.* 8: 430–437.
17. Chen, H., D. Ricklin, M. Hammel, B. L. Garcia, W. J. McWhorter, G. Sfyroera, Y. Q. Wu, A. Tzekou, S. Li, B. V. Geisbrecht, et al. 2010. Allosteric inhibition of complement function by a staphylococcal immune evasion protein. *Proc. Natl. Acad. Sci. USA* 107: 17621–17626.
18. Hammel, M., G. Sfyroera, S. Pyrpassopoulos, D. Ricklin, K. X. Ramyar, M. Pop, Z. Jin, J. D. Lambris, and B. V. Geisbrecht. 2007. Characterization of Ehp, a secreted complement inhibitory protein from Staphylococcus aureus. *J. Biol. Chem.* 282: 30051–30061.
19. Ricklin, D., A. Tzekou, B. L. Garcia, M. Hammel, W. J. McWhorter, G. Sfyroera, Y.-Q. Wu, V. M. Holers, A. P. Herbert, P. N. Barlow, et al. 2009. A molecular insight into complement evasion by the staphylococcal complement inhibitor protein family. *J. Immunol.* 183: 2565–2574.
20. Garcia, B. L., B. J. Summers, Z. Lin, K. X. Ramyar, D. Ricklin, D. V. Kamath, Z. Q. Fu, J. D. Lambris, and B. V. Geisbrecht. 2012. Diversity in the C3b [corrected] contact residues and tertiary structures of the staphylococcal complement inhibitor (SCIN) protein family. [Published erratum appears in 2012 *J. Biol. Chem.* 287: 9329.] *J. Biol. Chem.* 287: 628–640.
21. Garcia, B. L., K. X. Ramyar, A. Tzekou, D. Ricklin, W. J. McWhorter, J. D. Lambris, and B. V. Geisbrecht. 2010. Molecular basis for complement recognition and inhibition determined by crystallographic studies of the staphylococcal complement inhibitor (SCIN) bound to C3c and C3b. *J. Mol. Biol.* 402: 17–29.
22. Rooijakkers, S. H., J. Wu, M. Ruyken, R. van Domselaar, K. L. Planken, A. Tzekou, D. Ricklin, J. D. Lambris, B. J. Janssen, J. A. van Strijp, and P. Gros. 2009. Structural and functional implications of the alternative complement pathway C3 convertase stabilized by a staphylococcal inhibitor. *Nat. Immunol.* 10: 721–727.
23. Milder, F. J., L. Gomes, A. Schouten, B. J. Janssen, E. G. Huizinga, R. A. Romijn, W. Hemrika, A. Roos, M. R. Daha, and P. Gros. 2007. Factor B structure provides insights into activation of the central protease of the complement system. *Nat. Struct. Mol. Biol.* 14: 224–228.
24. Pryzdial, E. L., and D. E. Isenman. 1987. Alternative complement pathway activation fragment Ba binds to C3b. Evidence that formation of the factor B-C3b complex involves two discrete points of contact. *J. Biol. Chem.* 262: 1519–1525.
25. Forneris, F., D. Ricklin, J. Wu, A. Tzekou, R. S. Wallace, J. D. Lambris, and P. Gros. 2010. Structures of C3b in complex with factors B and D give insight into complement convertase formation. *Science* 330: 1816–1820.

26. Bunka, D. H., and P. G. Stockley. 2006. Aptamers come of age - at last. *Nat. Rev. Microbiol.* 4: 588–596.
27. Tuerk, C., and L. Gold. 1990. Systematic evolution of ligands by exponential enrichment: RNA ligands to bacteriophage T4 DNA polymerase. *Science* 249: 505–510.
28. Ellington, A. D., and J. W. Szostak. 1990. In vitro selection of RNA molecules that bind specific ligands. *Nature* 346: 818–822.
29. Gold, L., D. Ayers, J. Bertino, C. Bock, A. Bock, E. N. Brody, J. Carter, A. B. Dalby, B. E. Eaton, T. Fitzwater, et al. 2010. Aptamer-based multiplexed proteomic technology for biomarker discovery. *PLoS One* 5: e15004.
30. Vaught, J. D., C. Bock, J. Carter, T. Fitzwater, M. Otis, D. Schneider, J. Rolando, S. Waugh, S. K. Wilcox, and B. E. Eaton. 2010. Expanding the chemistry of DNA for in vitro selection. *J. Am. Chem. Soc.* 132: 4141–4151.
31. Davies, D. R., A. D. Gelinas, C. Zhang, J. C. Rohloff, J. D. Carter, D. O'Connell, S. M. Waugh, S. K. Wolk, W. S. Mayfield, A. B. Burgin, et al. 2012. Unique motifs and hydrophobic interactions shape the binding of modified DNA ligands to protein targets. *Proc. Natl. Acad. Sci. USA* 109: 19971–19976.
32. Caruthers, M. H., A. D. Barone, S. L. Beaucage, D. R. Dodds, E. F. Fisher, L. J. McBride, M. Matteucci, Z. Stabinsky, and J. Y. Tang. 1987. Chemical synthesis of deoxyoligonucleotides by the phosphoramidite method. *Methods Enzymol.* 154: 287–313.
33. Rohloff, J. C., A. D. Gelinas, T. C. Jarvis, U. A. Ochsner, D. J. Schneider, L. Gold, and N. Janjic. 2014. Nucleic acid ligands with protein-like side chains: modified aptamers and their use as diagnostic and therapeutic agents. *Mol. Ther. Nucleic Acids* 3: e201.
34. Gupta, S., M. Hirota, S. M. Waugh, I. Murakami, T. Suzuki, M. Muraguchi, M. Shibamori, Y. Ishikawa, T. C. Jarvis, J. D. Carter, et al. 2014. Chemically modified DNA aptamers bind interleukin-6 with high affinity and inhibit signaling by blocking its interaction with interleukin-6 receptor. *J. Biol. Chem.* 289: 8706–8719.
35. Otwinowski, Z., and W. Minor. 1997. Processing of X-ray diffraction data collected in oscillation mode. *Methods Enzymol.* 276: 307–326.
36. McCoy, A. J., R. W. Grosse-Kunstleve, P. D. Adams, M. D. Winn, L. C. Storoni, and R. J. Read. 2007. Phaser crystallographic software. *J. Appl. Cryst.* 40: 658–674.
37. Adams, P. D., R. W. Grosse-Kunstleve, L.-W. Hung, T. R. Ioerger, A. J. McCoy, N. W. Moriarty, R. J. Read, J. C. Sacchettini, N. K. Sauter, and T. C. Terwilliger. 2002. PHENIX: building new software for automated crystallographic structure determination. *Acta Crystallogr. D Biol. Crystallogr.* 58: 1948–1954.
38. Adams, P. D., P. V. Afonine, G. Bunkóczi, V. B. Chen, I. W. Davis, N. Echols, J. J. Headd, L. W. Hung, G. J. Kapral, R. W. Grosse-Kunstleve, et al. 2010. PHENIX: a comprehensive Python-based system for macromolecular structure solution. *Acta Crystallogr. D Biol. Crystallogr.* 66: 213–221.
39. Garcia, B. L., D. A. Skaff, A. Chatterjee, A. Hanning, J. K. Walker, G. J. Wyckoff, and B. V. Geisbrecht. 2017. Identification of C3b-binding small-molecule complement inhibitors using cheminformatics. *J. Immunol.* 198: 3705–3718.
40. Krissinel, E., and K. Henrick. 2007. Inference of macromolecular assemblies from crystalline state. *J. Mol. Biol.* 372: 774–797.
41. Wallace, A. C., R. A. Laskowski, and J. M. Thornton. 1995. LIGPLOT: a program to generate schematic diagrams of protein-ligand interactions. *Protein Eng.* 8: 127–134.
42. Gawande, B. N., J. C. Rohloff, J. D. Carter, I. von Carlowitz, C. Zhang, D. J. Schneider, and N. Janjic. 2017. Selection of DNA aptamers with two modified bases. *Proc. Natl. Acad. Sci. USA* 114: 2898–2903.
43. Drolet, D. W., L. S. Green, L. Gold, and N. Janjic. 2016. Fit for the eye: aptamers in ocular disorders. *Nucleic Acid Ther.* 26: 127–146.
44. de Jong, N. W. M., M. Vrieling, B. L. Garcia, G. Koop, M. Brettmann, P. C. Aerts, M. Ruyken, J. A. G. van Strijp, M. Holmes, E. M. Harrison, et al. 2018. Identification of a staphylococcal complement inhibitor with broad host specificity in equid *Staphylococcus aureus* strains. *J. Biol. Chem.* 293: 4468–4477.
45. Volanakis, J. E., S. R. Barnum, and J. M. Kilpatrick. 1993. Purification and properties of human factor D. *Methods Enzymol.* 223: 82–97.
46. Gelinas, A. D., D. R. Davies, and N. Janjic. 2016. Embracing proteins: structural themes in aptamer-protein complexes. *Curr. Opin. Struct. Biol.* 36: 122–132.
47. Ren, X., A. D. Gelinas, I. von Carlowitz, N. Janjic, and A. M. Pyle. 2017. Structural basis for IL-1α recognition by a modified DNA aptamer that specifically inhibits IL-1α signaling. *Nat. Commun.* 8: 810.
48. Thurman, J. M., and V. M. Holers. 2006. The central role of the alternative complement pathway in human disease. *J. Immunol.* 176: 1305–1310.
49. Alsenz, J., J. D. Becherer, B. Nilsson, and J. D. Lambris. 1990. Structural and functional analysis of C3 using monoclonal antibodies. *Curr. Top. Microbiol. Immunol.* 153: 235–248.
50. Qu, H., D. Ricklin, H. Bai, H. Chen, E. S. Reis, M. Maciejewski, A. Tzekou, R. A. DeAngelis, R. R. Resuello, F. Lupu, et al. 2013. New analogs of the clinical complement inhibitor compstatin with subnanomolar affinity and enhanced pharmacokinetic properties. *Immunobiology* 218: 496–505.
51. Schubart, A., K. Anderson, N. Mainolfi, H. Sellner, T. Ehara, C. M. Adams, A. Mac Sweeney, S.-M. Liao, M. Crowley, A. Littlewood-Evans, et al. 2019. Small-molecule factor B inhibitor for the treatment of complement-mediated diseases. *Proc. Natl. Acad. Sci. USA* 116: 7926–7931.
52. Thurman, J. M., D. M. Kraus, G. Girardi, D. Hourcade, H. J. Kang, P. A. Royer, L. M. Mitchell, P. C. Giclas, J. Salmon, G. Gilkeson, and V. M. Holers. 2005. A novel inhibitor of the alternative complement pathway prevents antiphospholipid antibody-induced pregnancy loss in mice. *Mol. Immunol.* 42: 87–97.
53. Subías, M., A. Tortajada, S. Gastoldi, M. Galbusera, A. López-Perrote, L. J. Lopez, F. A. González-Fernández, A. Villegas-Martínez, M. Dominguez, O. Llorca, et al. 2014. A novel antibody against human factor B that blocks formation of the C3bB proconvertase and inhibits complement activation in disease models. *J. Immunol.* 193: 5567–5575.
54. Williams, S. A., M. Kivimaki, C. Langenberg, A. D. Hingorani, J. P. Casas, C. Bouchard, C. Jonasson, M. A. Sarzynski, M. J. Shipley, L. Alexander, et al. 2019. Plasma protein patterns as comprehensive indicators of health. *Nat. Med.* 25: 1851–1857.